Low-order Modelling of the Light-round Ignition Transient in a Premixed Annular Combustor

R. Ciardiello[a], L. C. C. Mesquita[a] and E. Mastorakos[a]

[a]Department of Engineering, University of Cambridge, Cambridge, UK

ARTICLE HISTORY
Compiled January 5, 2022

ABSTRACT
This work presents a series of simulations of the light-round process in a premixed annular combustor, consisting of 18 individual swirl bluff body burners, using improvements to the previously-published stochastic low-order model SPINTHIR that mimics flame propagation with a Langevin particle model and continuous new particle generation. The improvements presented include the effect of dilatation and a stochastic component to the quenching criterion, resulting in capturing reasonably well the bending behaviour of the turbulent flame speed with turbulent intensity. The results showed that the light-round mechanism was well reproduced compared to experiments. The various versions of the model captured the trend of light-round time τ_{LR} as a function of the mixture's laminar flame speed with different degrees of accuracy. Overall, the results here reported improve our low-order capability to model the ignition transient in complex multi-burner configurations, which can help the design process of gas turbine combustors.

KEYWORDS
SPINTHIR; Low-order simulations; Light-round; Annular combustor; Ignition

1. Introduction

The development of lean-burning combustors for aircraft propulsion requires understanding of the ignition process [1]. In particular, high-altitude relight is subject to challenging conditions in a low-pressure, low-temperature environment with a large spectrum of parameter variation [2]. As a result, the design process usually involves trial and error testing of the specific geometry. Ignition is usually achieved by depositing a large amount of energy locally to cause the initiation of a flame kernel and lead to the full burning flame [3]. The ignition transient can be divided in four phases [4, 5]: (i) flame kernel formation, (ii) flame growth, (iii) flame stabilisation over a single burner and (iv) burner-to-burner propagation, known as "light-round". The light-round process can only be detected in multi-burner configurations, which are commonly employed in practice [1].

To rationalise and reduce the cost of the combustor design process, better physical understanding of the underlying processes and numerical simulations of the ignition transient are necessary. The light-round process has been recently experimentally investigated in premixed [6–9], non-premixed [10, 11] and spray [12–16] multi-burner

CONTACT R. Ciardiello Email: ciardiello.roberto@gmail.com

combustors, in linear or annular arrangements. Attempts to simulate the ignition transient in complex geometries through Large-Eddy Simulations (LES) have been carried out [15, 17–19]. These simulations provide precious insight on the physics of the flame front propagation, as they provide access to data not possible to be measured from experiments. However, such simulations are very expensive [17]. Further, even if the stochastic nature of the ignition transient in turbulent flames [4, 5] are being progressively integrated into the spark models in LES [20–23], this methodology still would require performing several independent simulations of light-round, hence still imposing an elevated computational cost. An alternative is to decouple the flame propagation transient from the flow simulation by developing a low-order model that can independently evaluate ignition probability. These models allow performing numerous tests of the ignition process starting from a flow-field obtained from the computational fluid dynamics (CFD) cold flow solution. The advantage is being able to collect statistically meaningful data with low computational cost. However, the model needs validation with experimental/DNS data and the accuracy should be carefully assessed.

An early attempt of low-order modelling of turbulent combustion was based on a "cellular automaton" algorithm, aiming to simulate the effect of turbulent movement on the flamelet propagation [24]. Adapting this concept to model the ignition of a combustor, Neophytou et al. [25] developed the code SPINTHIR, which stands for Stochastic Particle INTegrator for HIgh altitude Relight. SPINTHIR was the evolution of ideas suggested by Richardson [26] and the basic principle is to follow the flame propagation by generating particles to mimic the flame kernels, using a Monte Carlo method. Each particle moved inside the combustion chamber according to a simplified Langevin model [27] and to the flow field inside the burner. The flow field was an input coming from an averaged CFD cold flow solution. Thus, only one expensive CFD was required. A key feature of the model is the generation of new "flame particles" if at a certain point in space the mixture is flammable and the turbulent intensity is below some critical value associated with local extinction. This extinction criterion was based on the local Karlovitz (Ka) number, such that if a particle experienced $Ka > Ka_{cr}$ it was considered quenched. The Ka_{cr} was generally retrieved from experimental work on gaseous premixed flames [28] and set to 1.5. The calculation of Ka was based on the CFD-provided turbulent kinetic energy and the mixture's laminar burning velocity S_L. Here, this assumption is revisited to include a stochastic component to the individual particle's Ka, with the result of improving the physical fidelity of the results, as will be shown in this paper.

SPINTHIR was successfully applied to a wide range of non-premixed and spray flames by Neophytou et al. [25], capturing reasonably well the ignition probability spatial distributions in bluff body [29] and counterflow [30] non-premixed methane flames and in a swirling spray n-heptane flame [31]. The range of applicability was further tested on a Rolls-Royce aero-engine combustor [32]. The spark location and size were varied across the chamber and, in agreement with experiments [33], the most favourable locations for the spark were at the maximum width of the recirculation zone. Soworka et al. [34] extended the investigation to another Rolls-Royce combustor and provided an estimate of the lean ignition limits of the combustor. Finally, Cordier et al [35] proposed a modified version of the model to simulate a swirling flame, introducing a new criterion for flame propagation (based of particle growth) including a contribution of the laminar flame speed of the mixture. The results showed fair agreement between simulations and experiments, in terms of ignition probability contour and flame propagation patterns.

Sitte et al. [36] simulated the ignition transient in an unconfined premixed bluff body

stabilised flame. A few modifications were implemented, the main one was to use a local definition of the velocity fluctuations (u') to calculate the particle's Ka. The model was able to provide a good estimate of the turbulent flame speed for the canonical case of the freely-propagating turbulent flame, building confidence in the fundamentals of the model for premixed systems. The ignition simulations were in agreement with experiments performed on the same configuration, qualitatively capturing the flame propagation pattern and the ignition probability spatial distributions.

Only a few preliminary investigations have been carried out regarding the use of the low-order model for multi-burner configurations such as a non-premixed linear combustor [11] and a non-premixed annular combustor [37]. The stochasticity of the process was captured well in the simulations. Moreover, the light-round speed was the same order of magnitude as in the experiments and the shape of the propagating flame resembled the experimental observations.

While the aforementioned studies provided useful data for the validation of the code in non-premixed and spray configurations, the possibility to simulate the ignition transient in premixed combustors needs further investigation. The consensus in the literature from experiments and LES is that dilatation and turbulent flame propagation are both important for determining the flame position relative to a fixed coordinate system [12–19, 38–41]. The inclusion of all physical phenomena (dilatation, turbulent flame propagation, possibility of local extinction) in low-order models is important for building confidence in their results, but this has not been attempted systematically yet.

The aim of this work is to assess model improvements in SPINTHIR capturing dilatation and stochastic quenching in the context of the light-round behaviour in a premixed annular combustor. This will be achieved by carrying out a series of simulations using the original model from Ref. [25] and three modified versions, which are proposed in order to improve the capability of the code of reproducing premixed flame propagation. The results obtained will be compared to our previous experimental work on light-round, which provided a data set for model validation [9] and in particular data with different fuels and equivalence ratios giving hence a different laminar burning velocity and therefore propensity to local extinction for a given flow field.

2. Numerical modelling, setup and methodology

This section first presents a description of the low-order model SPINTHIR. Then, new modifications of the code are proposed and described, followed by the numerical setup and the conditions chosen for the simulations. Finally, the methodology for data processing is discussed.

2.1. Low-order modelling: SPHINTIR

Simulations of the ignition transient within an annular combustor were performed using the code SPINTHIR, introduced in section 1. In this work, the original code was slightly modified to improve its capability of simulating premixed flame propagation, as will be discussed in Section 2.2. An overview of the algorithm of the model is reported here.

The code first divides the combustion chamber in regular cells, equally distributed in a Cartesian grid, to simplify particle tracking. Each cell has four possible states: (i) cold, (ii) burning, (iii) quenched and (iv) out of domain. Cells inside the domain

are initiated as cold. Particles outside the borders of the annular chamber were set to out of domain, to reduce the number of particles and the computational cost. Then the spark location inside the grid is defined. The simulation starts by turning the state of the cells inside the spark domain to burning. Each burning cell releases a burning particle. Burning particles move according to a simplified Langevin model [27] described by the following equations:

$$dX_{p,i} = U_{p,i}dt \tag{1}$$

$$dU_{p,i} = -\left(\frac{1}{2} + \frac{3}{4}C_0\right)\omega_i(U_{p,i} - \tilde{U_i})dt + (C_0\epsilon_i dt)^{1/2}N_{p,i} \tag{2}$$

where $dX_{p,i}$ is the particle displacement in the interval dt, $\tilde{U_i}$ is the local Favre averaged velocity, C_0 is a constant equal to 2, $\omega_p = u'_p/L_{turb,p}$, u'_p is the velocity fluctuation, $L_{turb,p}$ is the turbulent length scale, ϵ_p is the local rate of dissipation of turbulent kinetic energy and $N_{p,i}$ is a stochastic variable following a gaussian distribution with zero mean and unity variance. The stochasticity in the process is simulated using the stochastic variables. The randomiser within the code was tested and improved compared to previous works [25, 36]. Equation 2 is made of a linear drift term towards the mean velocity and of an isotropic diffusion term. The random variable in each direction and for each particle is independent, thus particles are simply convected by the turbulent flow and their dispersion is modelled as a random walk.

When a particle moves inside a cold cell, the latter is turned to burning state and releases a new burning particle. The new burning particles will then move according to the Eqs. 1 and 2. Flame propagation is limited by the possibility of quenching inside the combustor. An extinction criteria was implemented into the model to capture this important aspect in turbulent flames. Particles move to a quenched state, and therefore stop moving, if the local Karlovitz number Ka_p exceeds a critical value. The Ka_p is calculated with the formula from Abdel-Gayed and Bradley:

$$Ka_p = 0.157\left(\nu\frac{(u'_i)^3}{L_{turb,i}}\right)^{1/2}\frac{1}{{S_{L,i}}^2} \tag{3}$$

where $S_{L,p}$ is the laminar flame speed at the particle location. The critical value for Ka_p was chosen following the experiments in Ref.[42] as $\mathrm{Ka}_{CR} = 1.5$, a widely-accepted result in premixed combustion. In addition to quenching, if a particle ends its movement outside of the combustion chamber, its status is shifted to out of domain and stops moving (and thus is not computed by the code anymore).

2.2. Modifications

As it will be later detailed in this work, the original SPINTHIR code fails to reproduce the experimental trends of light-round time in function of laminar flame speed observed by Ciardielo et al. [9]. Three modifications of the code are then here considered to overcome this limitation: (i) inclusion of a contribution of S_L and dilatation

in the particle velocity, (ii) changing the calculation of Ka by considering the velocity fluctuations experienced by the particles during their movement, following the procedure introduced by Sitte et al. [36] and (iii) a combination of both implementations.

Following the first path, the contribution of flame speed and dilatation to particle velocity was assumed to be linear. This led to a redefinition of the describing equation for U_p (see eq. 2 for reference), here reported:

$$dU_{p,i} = -\left(\frac{1}{2} + \frac{3}{4}C_0\right)\omega_i\left((U_{p,i} - \tilde{U}_i) \pm (S_{L,i}\frac{\rho_{ub}}{\rho_b})\right)dt + (C_0\epsilon_p dt)^{1/2}N_{p,i} \tag{4}$$

where ρ_{ub}/ρ_b is the density ratio between unburned and burned gases. Note that the new term in the equation was written in the code such that it was always added to the particle velocity drift term, being positive or negative depending on the direction of the flow. The choice is linked to the nature of premixed flame propagation which does not favour any direction and was modelled to act as an enhancement term for particle velocity.

The second option was to include the implementations presented in the work of Sitte et al. [36]. The authors proposed to change eq. 3 for a premixed flame. Instead of considering the u_i' coming from the CFD cold flow solution, the velocity fluctuation of the particle was obtained from the particle velocity during the simulation. A new variable denoted as instantaneous velocity fluctuation ($u_{inst,p}'$) can be defined as:

$$u_{inst,p}' = \sqrt{(U_{p,x} - \tilde{U}_x)^2 + (U_{p,y} - \tilde{U}_y)^2 + (U_{p,z} - \tilde{U}_z)^2} \tag{5}$$

thus the Ka_p was estimated as:

$$Ka_p = 0.157\left(\nu\frac{(u_{inst,p}')^3}{L_{turb,i}}\right)^{1/2}\frac{1}{{S_{L,i}}^2} \tag{6}$$

In non-premixed flames, flame propagation is connected to the presence of flammable mixture and depends on the mixture fraction fluctuations inside the flow. Oppositely, in premixed flame propagation, the equivalence ratio is constant throughout the system. Thus, considering a u' coming from the CFD solution in a certain zone would mean all particles passing through that region would experience the same Ka_p which could reduce the stochasticity in the model. The use of $u_{inst,p}'$ instead of u_i' could be a way to overcome this issue. The particle would be considered to experience the velocity fluctuations related to their random walk instead of the one coming from the cold flow value at the local cell.

The third option examined was to implement both modifications in the code. Namely, particle velocity was enhanced by the term introduced in eq. 4 and the Ka_p was calculated using eq. 6. The new three variants of SPINTHIR presented will be hereafter defined as: (i) "version 1", (ii) "version 2" and (iii) "version 3", respectively.

2.3. Geometry and operating conditions

The simulated geometry was a numerical replication of the annular combustor from the experiments in Refs. [9, 43]. In particular, the experiments of our previous work in Ref. [9] will be used to compare and validate the results from the simulations. A detailed description of the experimental apparatus can be found in Refs. [9, 43, 44], thus only a brief description of the combustion chamber is reported here. The annular combustor comprised of 18 individual swirl bluff body stabilised burners. Each burner was a cylindrical pipe (150 mm long, with an inner diameter of D_b= 18.9 mm) centrally fitted with a conical bluff body (with a diameter of $D = 13$ mm and half angle of 45°). This arrangement resulted in a blockage ratio of ∼47% at the exit of each burner. A swirler (exit vane angle $\alpha = 60°$) was placed upstream of the bluff bodies, generating an anti-clockwise tangential flow in the chamber with a geometrical swirl number of 1.22 [45]. The annular combustion chamber was delimited by two concentric walls with a diameter of $D_{inner} = 127$ mm and $D_{outer} = 203$ mm, for the inner and outer boundaries, respectively.

The flow conditions simulated are reported in Table 1. These are varied in the code by imposing the value of the local S_L of the mixture, uniform throughout the combustion chamber as the burner was operated in premixed mode. The spark volume was defined as a cube with length of 6 mm, resulting in 8 particles being turned to burning to initiate the ignition test. The size of the spark domain was chosen to resemble the experimental observations [9]. The spark was located either close to the bluff body at an axial distance of $x/D = 0.5$ from the bluff body or in the middle of the combustion chamber at an axial distance of $x/D = 5$ from the bluff body, where D is the bluff body diameter. The operating conditions were chosen in order to match the experiments in Ref. [9].

Table 1.: Flow conditions of the test cases

# burners	Fuel	U_{mix}	ϕ	S_L (cm/s)	Spark location [x/D]
18	CH_4	16	0.75-0.85-1	24-30-36	0.5 and 5
18	C_2H_4	16	0.58-0.62-0.67- 0.77-0.80-0.86-0.90	24-30-36- 47-50-56-59	0.5 and 5

The last parameters to be specified in the code are the time step (Δt) and the grid size (ΔX). In first instance, these quantities can be defined based on physical quantities inside the domain [25]. In particular, in order to capture the entire spectrum of timescales of turbulence, the Δt should not exceed the mean turbulent timescale T_{turb}, defined in eq. 7:

$$T_{turb} = \frac{L_{turb}}{u'} \tag{7}$$

The grid size should be larger than the smallest turbulence lenght-scale (Kolmogorov scale [27]). Moreover, the combination of (Δt) and (ΔX) should be chosen in order to prevent any particle to travel more than ΔX each time step. In other words, a particle should not jump a grid cell without entering it. This is an essential criterion for the applicability of this model, as it relies on the cell-by-cell travelling of the particles and on their local check of the conditions for flame propagation. A particle jumping

a cell may introduce inaccuracy, as it could be artificially increase the propagation of the flame or overestimate its quenching. From the Langevin equation in Eq. 2 this condition can be summarised as:

$$\Delta X_{max} = 2(C_0 \epsilon_p dt)^{1/2} \Delta t \tag{8}$$

The parameters chosen for the simulations were $\Delta t = 0.1$ ms and $\Delta X = 3$ mm. Both values influence the speed of the code and the computational cost. An assessment of the validity of the Δt is provided in the next subsection.

The simulations were performed on a desktop computer, 64-bit, Intel(R) Core(TM) i7-6700, CPU @3.40 GHz, 64 Gb RAM. The maximum time-step was 1600, resulting in 160 ms of simulation for each run. Depending on the flow conditions and on the specific model employed, each simulation was carried out in ∼45-60 minutes.

2.4. Grid size and timestep analysis

The grid size ΔX was fixed to 3 mm, as a trade-off between fine spatial discretisation and computational cost. The time-step can be initially selected following the suggestions reported in section 2.3, but a convergence analysis on Δt can be performed, using the light-round time (τ_{LR}) as the parameter for the comparison.

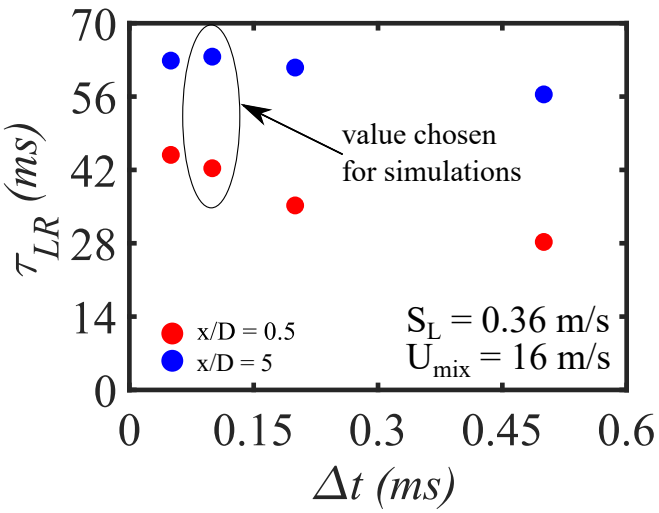

Figure 1.: Plot of τ_{LR} for various values of the timestep Δt. Operating conditions are $U_{mix} = 16$ m/s and $S_L = 0.30$ m/s. The times reported are averages of at least 10 independent runs.

Figure 1 displays the calculated τ_{LR} for the same operating conditions, running tests with a different choice of Δt. It is evident that an increase in Δt above 0.1 ms significantly reduced the observed τ_{LR}, especially when the spark was located close to the bluff body ($x/D = 0.5$). Thus, the timestep was set to $\Delta t = 0.1$ ms, to provide accurate measurements at a reasonable computational cost. The miscalculation of τ_{LR} because of a too large is caused by the lagrangian flame particles skipping a cell, reaching the next one without entering all the cells in the path. This jumping of cells represents an important source of error, as it causes an increasing miscalculation of the particle trajectory and of which cells should be ignited by this moving

particle, ultimately leading to wrong light-round times and ignition probability. It is, then, essential to prevent the lagrangian particles from jumping cells, which can occur when the particle velocity overcomes the limit represented by the ratio $\Delta X/\Delta t$. The aforementioned condition is usually quantified in CFD simulations by introducing the Courant-Friedrichs-Lewy (CFL) number, defined as:

$$CFL = \frac{u\Delta t}{\Delta X} \tag{9}$$

where u is the flow velocity. To ensure the reliability of the SPINTHIR simulations, the definition of ΔX and Δt should respect the condition:

$$CFL < 1 \tag{10}$$

Thus, this condition is here evaluated, with Fig. 2 showing the three components of the particle velocity at a random timestep, when fixing $\Delta t = 0.1$ ms. From the three plots it can be observed that the velocity of each particle does not exceed the ratio $\Delta X/\Delta t = 30$ m/s, reaching peaks ∼10-20 m/s. Therefore, the condition $CFL < 1$ is clearly satisfied for the values $\Delta X = 3$ mm and $\Delta t = 0.1$ ms used here, ensuring that the lagrangian particles will not jump any cells.

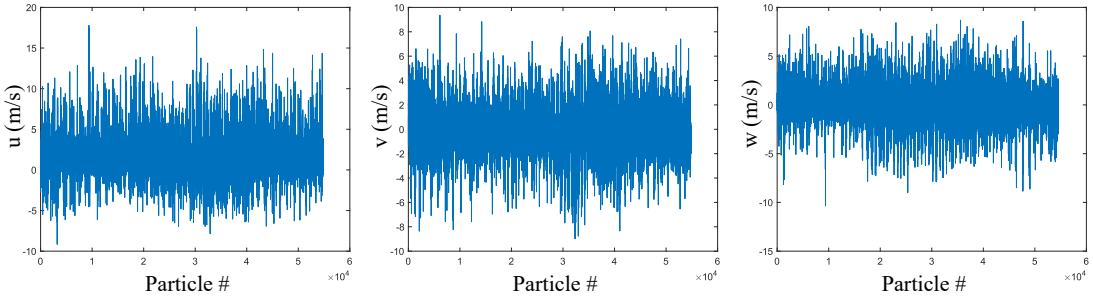

Figure 2.: Plots of the three components of the particle velocity (u,v and w) at a random timestep during an ignition test, with Δt fixed to 0.1 ms. Operating conditions are $U_{mix} = 16$ m/s and $S_L = 0.30$ m/s. The spark was located at $x/D = 0.5$.

2.5. Methodology for light round time calculation

At each time step a quantity denoted as "ignition progress factor" , Π, was defined as the ratio between the number of ignited cells and the total number of cells. The evolution of this number follows the progression of the flame front when moving across the chamber to ignite each individual burner. An example of Π in five individual successful events is reported in Fig. 3.

The images inserted in the plot provide a visualisation of the ignition transient for different positions along the ignition progress factor curve. The threshold for a successful ignition event was set to $\Pi = 0.6$, as it was seen that the typical light-round process was over at around $\Pi = 0.85$ and all the simulations reached a plateau around $\Pi = 0.94$. The reason why this factor did not reach unity is that the domain needed to be larger than the geometry (therefore 6% of cells cannot be ignited).

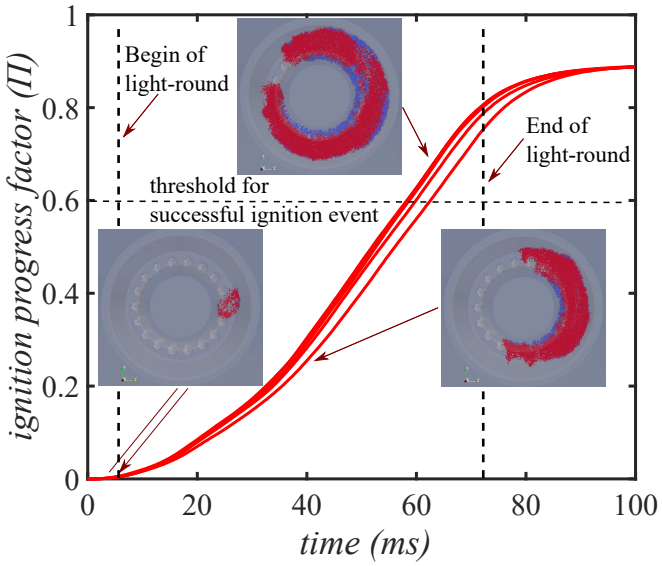

Figure 3.: Time evolution of the ignition progress factor for five ignition events, showing different phases of the light-round and the definition of light-round time.

The criterion for evaluating the light-round time was similar to the experimental one in Ref. [9], to provide a fair comparison. The beginning of the light-round transient was set to $\Pi = 0.01$. The end of the light-round process depended on the operating conditions, though in most cases it corresponded to $\Pi = 0.8$. These choices, albeit arbitrary, depended on an analysis of the images of the simulations for the different time steps compared to the OH^* images recorded in the annular combustor [9]. As for the experiments, this definition was necessary to remove the first three phases of the ignition transient from the ignition time, to properly investigate only the light-round time.

It should be noted that the experimentally-determined light-round time is based on line-of-sight imaging from downstream, allowing for the possibility that a burner remains unignited although there is visible flame at the same azimuthal location downstream. This suggests an under-estimate of the τ_{LR}. In the model, the possibility exists that the flame has not advanced to neighbourhood burners but it slowly filling-up cells associated with individual burners, suggesting an over-estimate of the true time of light-round. Therefore, when assessing the performance of the model the trends in τ_{LR} with operating condition are more important to consider than the exact quantitative values.

3. Results and discussion

3.1. CFD of the cold flow in the annular combustor

The CFD flow fields were obtained using the finite volume code PRECISE-UNS [46]. Steady RANS simulations were performed on the annular combustor to capture the time-averaged flow field. The simulation domain captures all of the chamber and the whole lenght of the bluff bodies, going sufficiently upstream of the swirlers, as shown in [9]. To reproduce all the cases relative to the investigation of light-round time in the 18-burner configuration reported in Ref. [9], only one converged CFD cold flow

simulation was required. A mass flow rate of air of $\dot{m} = 2.59$ g/s is specified, resulting in the $U_{mix} = 16$ m/s at the chamber entrance. The equivalence ratio of the experiment defines the S_L of the mixture used in SPINTHIR, set as uniform inside the chamber. Turbulence is modelled with a RANS RNG-k-epsilon model, and convective terms are discretised with a 2nd order central algorithm. Wall conditions are set to adiabatic and to slip. A large cylindrical region is added at the exit of the chamber to mimic the atmosphere. Pressure outlet conditions are applied at the exit of the chamber. Pressure is 1 atm and temperature is set to 293K and walls are considered adiabatic, as SPINTHIR does not consider thermal exchanges with the walls. The numerical mesh is fully unstructured and tetrahedral, refined inside the swirler, to correctly resolve the flow field in the small passages.

Figure 4 displays cut planes of the annular chamber, showing the axial component of the velocity field and the pseudo-stream lines from a burner. At the exit of a single burner the mixture axial velocity is close to 16 m/s, as expected from the imposed mass flow rate. As shown in Fig. 4a, the presence of a bluff body and a swirler and the interaction between adjacent flows resulted in the formation of two recirculation zones: (i) a central recirculation zone (CRZ), in the wake of the bluff body and (ii) a side recirculation zone (SRZ) in the inter-burner region. The CRZ extended for $\sim$1.5 D and the axial velocity was ~ -5 m/s (see Fig. 4c), while the SRZ was shorter ($\sim D$ tall) and characterised by a negative axial velocity of ~ -3 m/s. The swirler added upstream of the bluff body generated an anticlockwise tangential flow. Figures 4b and 4c present two cross-sectional cuts showing the axial velocity at the two positions where the kernel will be initiated. One can see that for the $x/D = 0.5$ case (Fig. 4b), the kernel is initiated inside the CRZ, while for the $x/D = 5$ case (Fig. 4c) the kernel is initiated just downstream of the CRZ, where the average flow has positive axial velocity. The tangential component of the velocity spans in magnitude between ~ -13 m/s and ~ 13 m/s, both in the CRZ and in the SRZ. Finally, Fig. 4d shows the flow pseudo-streamlines as initiated at the initial position of the ignition kernel. Some possible paths for the particles (as carried by the mean flow) are highlighted, showing either how they can be convected downstream or move from burner to burner, promoting the light-round.

3.2. Evaluation of turbulent flame speed in a canonical case

In order to provide a comparison on how accurately the new versions of the code can reproduce turbulent flame speed, a canonical case of freely propagating particles in a box was investigated. The procedure followed the one outlined by *Sitte et al.* [36]. A regular domain was created, in the form of a parallelopipedon with squares representing the inlet and the outlet of the domain. The dimensions of the box were chosen to be wide enough to limit boundary effects and set to $2\,L_T$ in width and $10\,L_T$ in length. L_T is the turbulent lenghtscale, which was set constant and equal to 0.03 m, to favour comparison with experimental data [28]. The box was filled with a quiescent uniform mixture of fuel and air, with a set ϕ (and thus S_L). As a result, particles inside the domain move according to a flow field due to non-decaying, uniform, isotropic turbulence. In other words, in the equation for the particle velocity, the mean velocity is set to 0 everywhere. The grid size was chosen to be 2 mm and the timestep was set to 0.1 ms. Simulations were carried out by varying the u' of the flow field and the S_L of the mixture (assumed to be constant everywhere).

The simulation was initiated by turning to burning all the particles placed on the

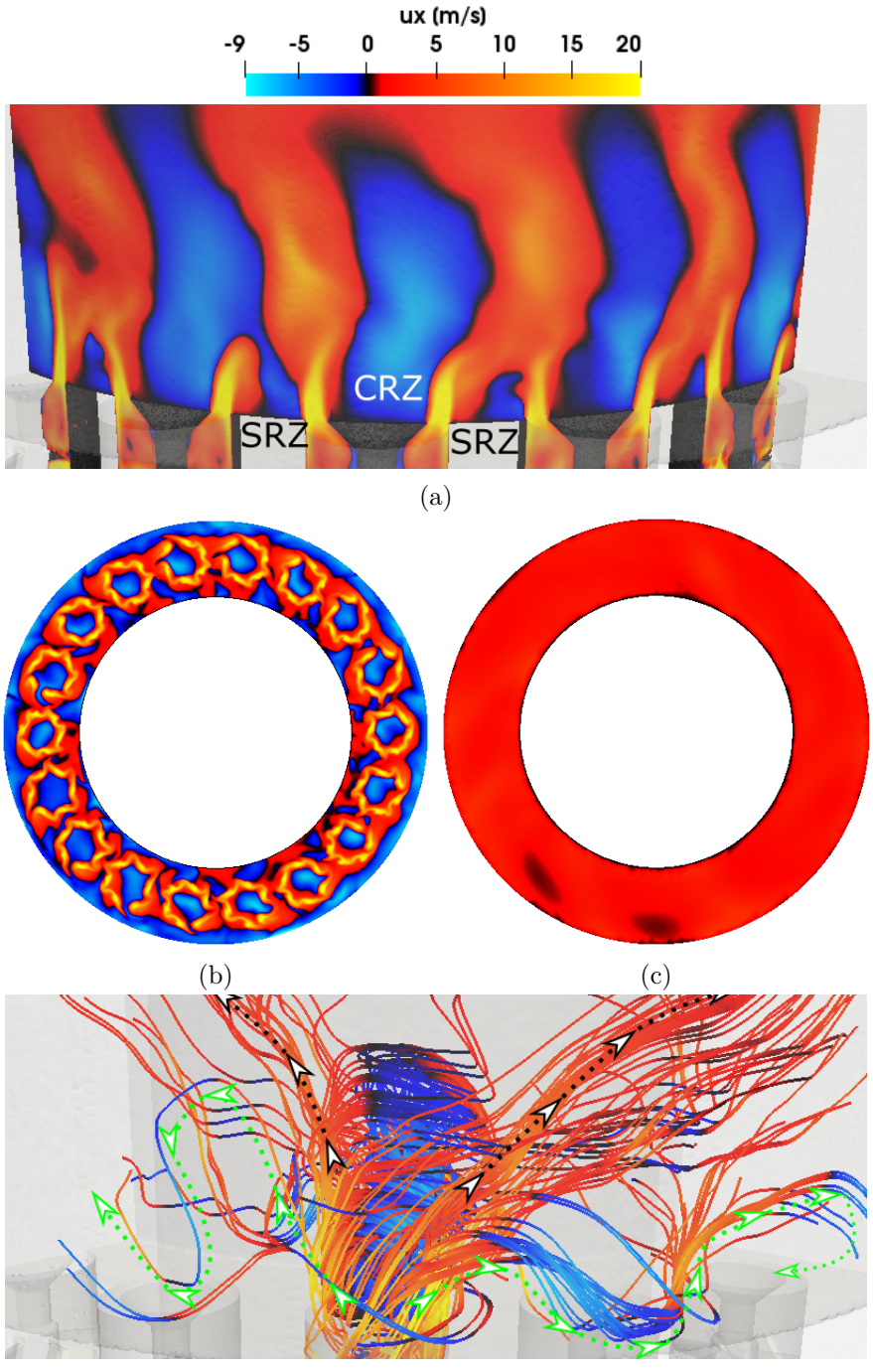

(a)

(b)

(c)

(d)

Figure 4.: RANS simulations: (a) Bluff-body mid-plane cut showing the axial velocity field, with the Central Recirculation Zone (CRZ) and Side Recirculation Zone (SRZ) in shades of blue. (b and c) Cross-section cuts at $x/D = 0.5$ and $x/D = 5$, respectively, showing the axial velocity fields at the positions where the kernels are initiated. (d) Pseudo streamlines showing the possible paths from particles initialized at the center of a bluff-body. The Purple arrows highlight possible paths where the particles go straight downstream, while the Green arrows highlight paths where the particles can move to ignite the mixture in the neighbouring injectors by the SRZ (right green path) or by the CRZ (left green path). Please contact authors if a scheme adapted to colour-blindness is needed.

inlet. Then, the particles started to move and propagate depending on the particle velocity equations and on the Ka extinction criterion employed. The different version of SPINTHIR employed influenced the particle path and the time it took to reach the other side of the domain.

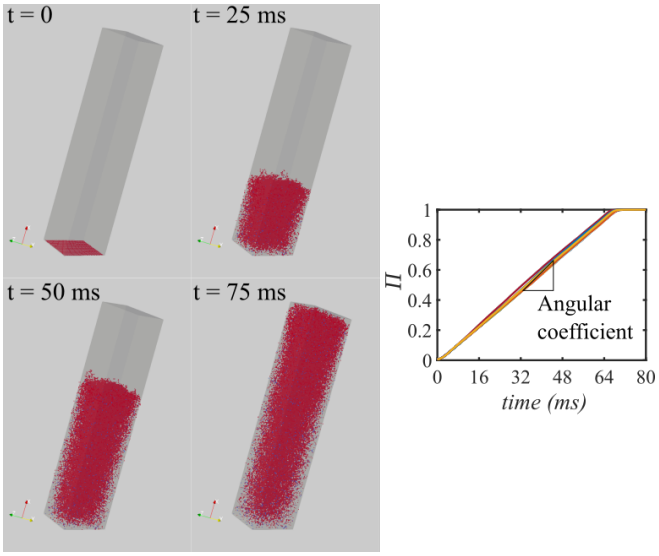

Figure 5.: Images of few timesteps of the particle propagation (left) and plot of the ignition progress factor (Π), for various runs (right). In this case the SPINTHIR version was number 2, $u' = 8$ m/s and $S_L = 0.24$ m/s.

Figure 5 shows an example of particle propagation inside the domain, along with the corresponding ignition progress factor plot. The particle motion inside the domain can be visualised from the images in the left-hand side in Fig. 5. From one side of the box ($t = 0$), particles propagate uniformly (see $t = 25$ ms and $t = 50$ ms) until reaching the end of the parallelepipedon ($t = 75$ ms). The evolution of the particle journey can be observed from the ignition progress factor. In particular, the slope of the curve appeared to be almost straight for $0.1 < \Pi < 0.9$. The end of the process corresponded to $\Pi = 1$ as, in contrast with the annular combustor, all particles were ignitable in this very simplified geometry. The mean particle velocity during their journey throughout the box was obtained from the angular coefficient of Π versus time (see the right-hand side of Fig. 5) and used to define a form of "virtual" turbulent flame speed. As previously mentioned, the angular coefficient was almost constant for a wide range of Π.

The resulting turbulent flame speeds calculated using the version of the code from Ref. [25] and the three variants of SPINTHIR, compared to experimental evidence from Ref. [28] are reported in Fig. 6. It is clear from the plot that the standard version of SPINTHIR is not capable of capturing the bending effect of the turbulent flame speed with the turbulence intensity, widely reported in the literature [47–50]. As L_T and u' are fixed inside the domain, the Ka_p calculated through eq. 3 is constant everywhere. Thus, particles either propagate, faster when using version 1 compared to the standard version due to the enhancement of U_p, or quench. As a result, the normalised S_T is observed to increase almost linearly until reaching a point where the S_T drops to zero as there was no propagation. This limit coincides with the flow conditions leading to Ka_p >1.5, which is the critical value for the extinction criterion

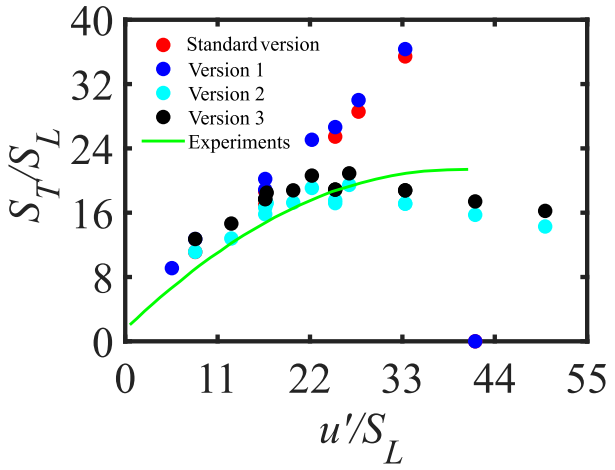

Figure 6.: Plot of turbulent flame speed (S_T) against u′, both normalised by the laminar flame speed of the mixture S_L. The experimental data are retrieved from the work of Abdel-Gayed et al. [28]. Each point represents the average of at least 10 independent tests.

employed. Below ~ 20 u'/S_L the simulated S_T/S_L was closer to the green curve (the experimental values from Ref. [28]).

In contrast, versions 2 and 3 performed better and displayed more accurate results. The simulated turbulent flame speed showed the same trends as the experimental one, especially for low/middle values of turbulence intensity. The new definition of Ka_p produced a unique value for each particle, instead of a fixed one for the entire mixture. This resulted in the possibility of particle quenching inside the domain and led to differences between the individual cases. As before, version 3, which included S_L in the particle velocity equation, resulted in a slightly higher S_T.

To summarise, the results indicated that version 2 and 3 are capable of reproducing the turbulent flame speed in premixed flame propagation, while the standard version from Ref. [25] and version 1 are accurate only for lower values of u'/S_L.

3.3. Simulation of the light-round transient

Simulations were carried out placing the spark close to the bluff body ($x/D = 0.5$) and in the middle of the combustion chamber ($x/D = 5$), similarly to the experiments in Ref. [9]. Figure 7 shows a view from downstream of the combustion chamber for the SPINTHIR results (using the version of the code from Ref.[25]), visualising the burning and quenched particles, and for OH* chemiluminescence from the experiments [9]. In both cases the kernel is initiated at the centre of the right-most bluff-body as shown in Fig. 7 (looking from the top). The azimuthal expansion of the flame is visible. In good agreement with the experimental observation, the flame edges on the inside wall and outside wall are well captured. This is due to the swirl influence on the flame propagation pattern near each of the burners. However, it is also evident that the flame edge has travelled the same distance at a longer time in the simulation compared to the experiment.

A more detailed comparison of the various model versions is now presented. Figure 8 reports a sequence of images of an ignition attempt when the initial spark was set

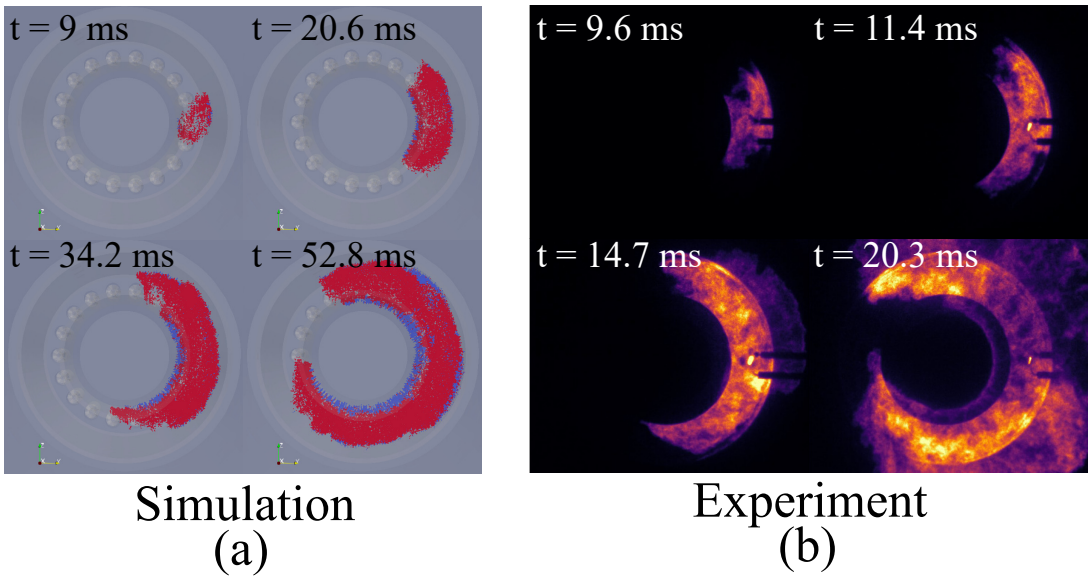

Figure 7.: Comparison between image sequences of ignited particles in simulations (a) and OH* chemiluminescence images of the light-round process. Experimental data are retrieved from [9]. Operating conditions are: $U_{mix} = 16$ m/s, $\phi = 0.75$ and spark longitudinal location is $x/D = 0.5$ and the fuel used is CH4. SPINTHIR version is the one retrieved from Ref. [25].

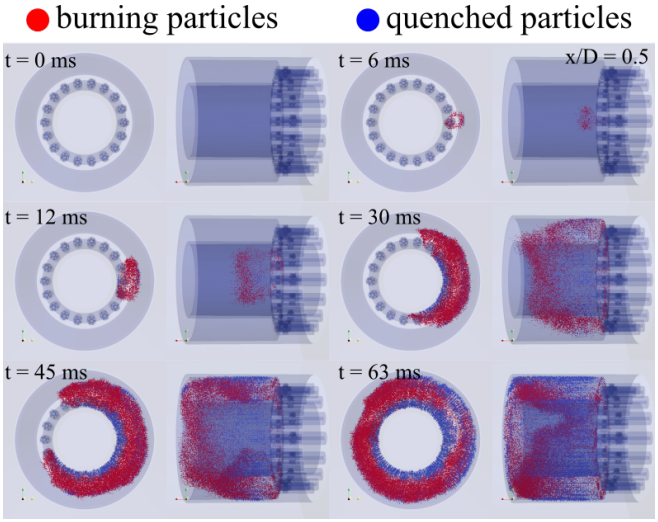

Figure 8.: Image sequence of an ignition event from the simulations with the version of SPINTHIR from Ref. [25]. Operating conditions are $U_{mix} = 16$ m/s and $S_L = 0.30$ m/s and the fuel used is CH4. The spark was located at $x/D = 0.5$. Burning particles are coloured in red, while quenched particles in blue.

at $x/D = 0.5$, using the version of SPINTHIR from Ref. [25]. From the initial volume, the particles started to move in the three directions (see $t = 6$ ms), propagating towards the adjacent burners (see $t = 12$ ms). The light-round proceeded forming two branches (see $t = 12$ ms and $t = 30$ ms), which preferentially followed the anti-clockwise swirl direction. In particular, the swirl-induced tangential component of the velocity

resulted in the anti-clockwise "flame" arch to propagate faster on the outer side of the combustion chamber and the clockwise one to lean towards the inner side of the chamber (see $t = 30$ ms and $t = 45$ ms). The light-round ended with the particle filling the entire chamber, when the two propagating arches merged on the opposite side of the spark volume region (see $t = 63$ ms). The simulations reproduced quite closely the experimental evidence in Ref. [9]. Some key elements are retrieved: (i) the propagation followed the formation of a kernel which expanded towards the adjacent burners, (ii) the propagating front formed two branches travelling around the combustion chamber, (iii) the flame front followed the swirl direction and leaned towards the inner or the outer side of the chamber and (iv) the end of the light-round consisted in the merging of the two branches on the other side of the spark volume region.

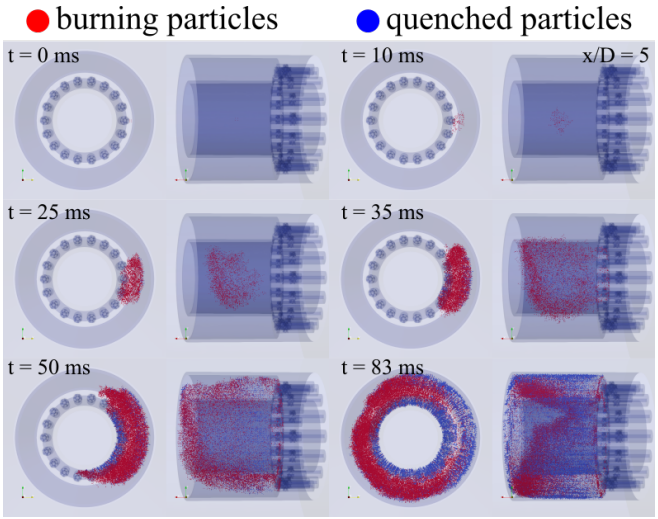

Figure 9.: Image sequence of an ignition event from the simulations with the version of SPINTHIR from Ref. [25]. Operating conditions are $U_{mix} = 16$ m/s and $S_L = 0.30$ m/s and the fuel used is CH4. The spark was located at $x/D = 5$. Burning particles are coloured in red, while quenched particles in blue.

The same correspondence in the mechanism of the ignition transient between simulations and experiments was found with a spark placed downstream in the combustion chamber, at $x/D = 5$, as shown in Fig. 9. From the initial spark volume, particles move simultaneously upstream against the mean flow and azimuthally across the chamber (see $t = 10$ ms and $t = 25$ ms). After reaching the bluff bodies aligned with the spark (see $t = 35$ ms), two flame branches form and start travelling across the chamber, following a pattern influenced by the swirl direction(see $t = 50$ ms), similarly to what observed for the case $x/D = 5$. Compared to the experimental observations in Ref. [9], the simulations managed to capture the key phenomena that were detected during the process. Namely: (i) peculiar propagation pattern from the downstream spark location (simultaneously upstream and azimuthally), (ii) ignition of the burners just upstream of the spark location, before the flame front started to sweep around the annular chamber and (iii) decrease in propagation speed compared to the case with the spark located close to the bluff body.

While the mechanism of the flame propagation was well captured in the simulations, the light-round time (τ_{LR}) did not match the experimental evidence in Ref. [9]. In particular, the standard code was not capable of capturing the trend of τ_{LR} with the

laminar flame speed of the mixture, as will be discussed in detail in the next section.

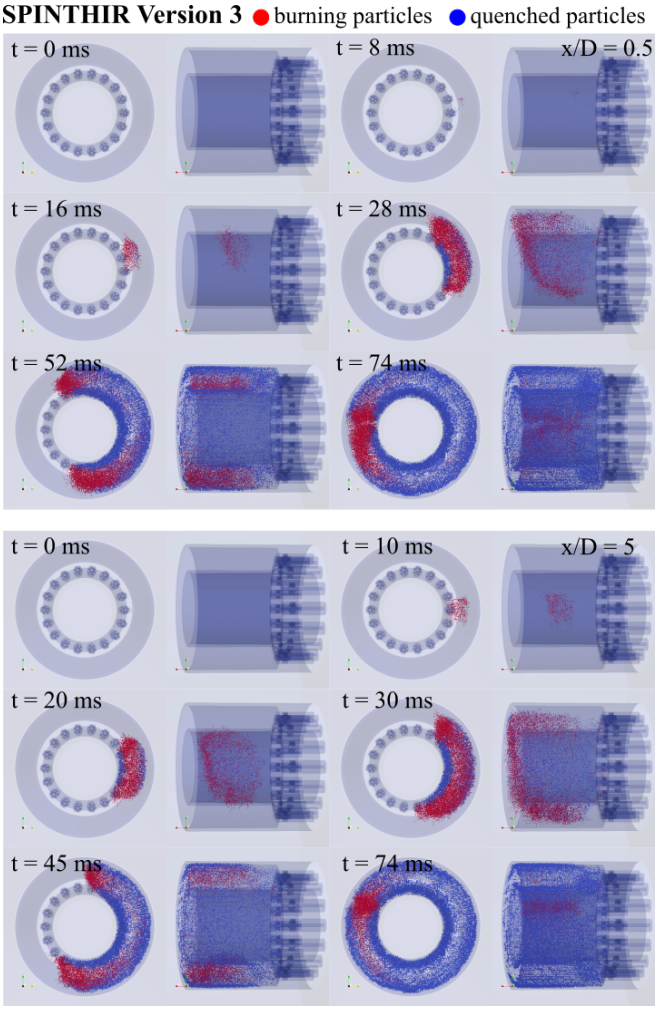

Figure 10.: Image sequence of an ignition event from the simulations using SPINTHIR version 3. Operating conditions are U_{mix} = 16 m/s and S_L = 0.30 m/s and the fuel used is CH4. The spark was located at x/D = 0.5 in the series at the top and at x/D = 5 in the series at the bottom. Burning particles are coloured in red, while quenched particles in blue.

Version 3 of the model was the one implementing most of the key physics of premixed flame propagation while keeping it simple and cost-effective. Therefore, we are showing simulations only with Version 3 for the sake of clarity and conciseness. Image sequences of the simulated ignition process are reported in Fig. 10. The use of a different definition of particle Ka resulted in more quenching inside the combustor and different propagation of burning particles. For the x/D = 0.5 case (Fig. 10 - top), the initial kernel got first convected downstream (see t = 8 and t = 16 ms) before starting to propagate towards the individual burners (see t = 28 ms) and eventually around the annular chamber (see t = 52 ms and see t = 74 ms). The simultaneous increase in particle velocity fluctuation and quenching (compared to the standard version of the code) resulted in a distortion of the flame front. The key features of the experiments in Ref. [9] can still be retrieved in the burner-to-burner propagation mechanism, even

if the beginning of the process is now quite different. When the S_L of the mixture was reduced it was found that the light-round would fail in some of the simulations using SPINTHIR versions 2 and 3. This is particularly relevant for the CH4, S_L = 0.24 m/s, $\phi = 0.75$, spark at $x/D = 0.5$ case, where only 10% of the cases resulted in a successful ignition. The reason was the extinction of the initial burning particles near the spark location a few milliseconds after the beginning of the simulation. This is in contrast with the experiments that showed that the ignition probability was $\sim$1 when $\phi > 0.68$ [43] and may be due to inaccuracy in the cold flow CFD solution that affect the initial propagation of the particles.

In case of a spark located at $x/D = 5$ (see the bottom image sequence in Fig. 10), particle movement presented strong similarities with the experimental results of Ref. [9]. From the initial kernel, particles were convected and started to propagate downstream (see $t = 10$ ms) as well as azimuthally (see $t = 20$ ms and $t = 30$ ms), eventually leading to the complete light-round (see $t = 45$ ms and $t = 74$ ms). The propagation appeared quite uniform, without a distinct upstream propagation towards the individual burners. This mechanism of propagation resulted in reduced differences between sparking at $x/D = 5$ and $x/D = 0.5$. In particular, the end of the light-round process is around the same time from the initial spark. Differences in the τ_{LR} between these two locations, shown in the next section, can be attributed to the time it took to form a kernel big enough to start the process (that is the length of Phases 1-3 of the ignition transient). Moreover, the accuracy of the cold flow CFD solution can also affect the reliability of the simulations. No failed attempts in the ignition trials were found when the spark was located downstream, what is also in agreement with the experiments.

3.4. Evaluation of the light-round time

Figure 11 presents the τ_{LR} obtained from the various SPINTHIR versions as a function of S_L compared to the experimental evidence from Ref. [9]. The results from the simulations with the version of SPINTHIR from Ref. [25] are displayed in Fig. 11a. In agreement with the experiments [9], it was found that the simulations with the standard SPINTHIR resulted in a longer light-round time when placing the spark downstream ($x/D = 5$), when compared to the simulations of $x/D = 0.5$ case. However, τ_{LR} is $\sim$3-4 times higher in the simulations compared to the experiments. Moreover, the key characteristic in the experimental trend was not retrieved: the correlation between τ_{LR} and S_L. In the simulations, the ignition time did not depend on the flame speed of the mixture, being almost constant for all the mixtures employed.

The explanation is related to the modelling of particle velocity: the Langevin equations do not take into account flame speed and dilatation, but give a particle motion that depends only on the turbulence. Thus, the model underestimates the flame velocity. Furthermore, the extinction criterion is not susceptible to small variations in the Ka number due to the variation in S_L. This may be due to the calculation of u' from the CFD flow field that might not reflect the degree of fluctuations the particles are actually exposed to.

Including S_L and dilatation (version 1) resulted in a decrease in light-round time, as it can be observed by comparing Figs. 11b and 11a. Moreover, the key observation of decreasing τ_{LR} with an increase in S_L was captured. Overall, the trends of the results from the simulations with SPINTHIR version 1 were in agreement with the experiments, with $\tau_{LR,sim} \sim 2\tau_{LR,exp}$.

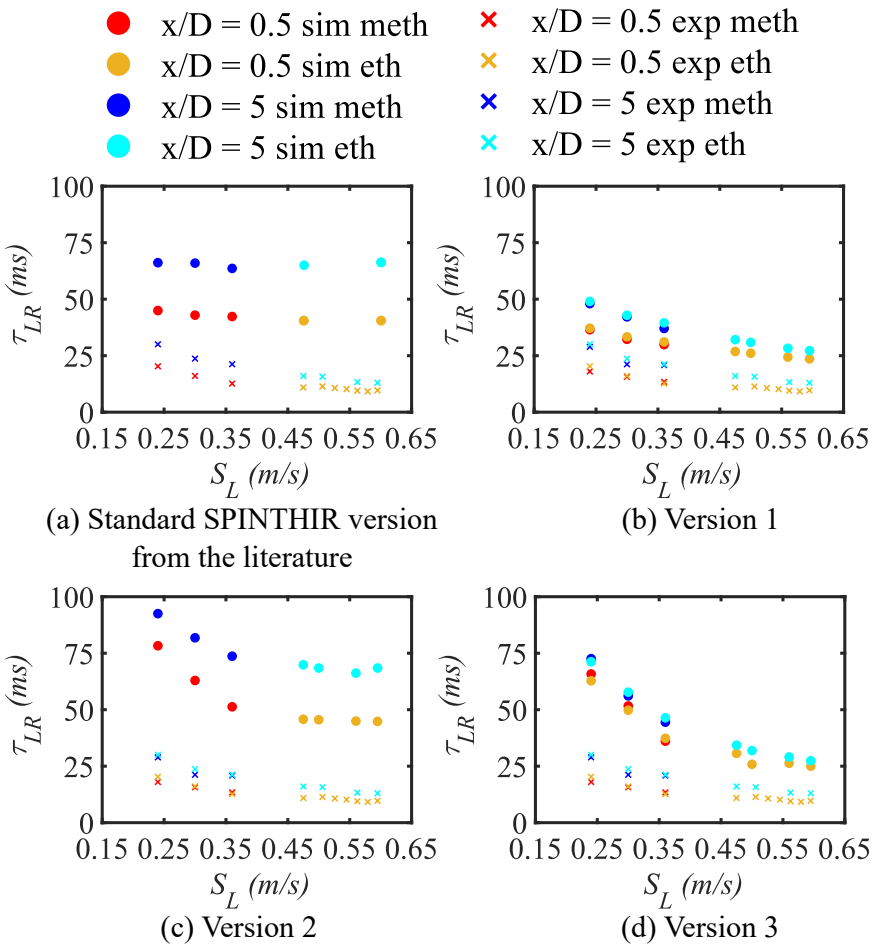

Figure 11.: τ_{LR} as a function of the S_L of the mixture for both CH4 and C2H4 for experiments and the simulations performed with SPINTHIR in four versions: version from Ref. [25] (a), version 1 (b), version 2 (c) and version 3 (d). In each plot the experimental results from Ref. [9] are added for comparison. Depending on the S_L and on ρ_{ub}/ρ_b (when implemented in the code) the fuel considered in the simulation was either methane or ethylene, similarly to the experimental campaign.

The results from version 2, presented in Fig. 11c show that the simulations were partially capable of reproducing the experimental results, in particular regarding the link between τ_{LR} and S_L. For low values of S_L, τ_{LR} decreased until reaching a plateau after $S_L = 0.47$ m/s. A plausible explanation is that increasing the mixture strength over a certain value compensated the quenching increase due to the new definition of Ka_p. As a result, the simulations from version 2 became close to the one with the standard version of SPINTHIR, which can also be observed by comparing Figs. 11c and 11a. For high values of S_L both versions reported similar τ_{LR}. As for the other characteristic, version 2 managed to capture the increase in τ_{LR} when moving the spark downstream, while the τ_{LR} was 3-4 times higher than the experimental values.

Finally, the correlation between τ_{LR} and S_L from the simulations with SPINTHIR version 3 is displayed in Fig. 11d. Similarly to version 1, τ_{LR} reduced when increasing S_L of the mixture. Also, as was previously discussed, the difference in light-round time between sparking at $x/D = 0.5$ and $x/D = 5$ is progressively lost as S_L is increased,

in line with the experiments. However, τ_{LR} was ~ 2 times greater compared to the experiments. A possible explanation for such discrepancies may be the influence of the accuracy of the CFD cold flow on the simulations with SPINTHIR. For all the three versions, the influence of the unburnt to burnt density ratio between the two fuels (which was only reflected in the dilatation factor) showed minor contribution compared to the influence of S_L, in agreement with the experiments.

3.5. Discussion: advantages and limitations

SPINTHIR was employed in four different variants to simulate the ignition transient in a premixed annular combustor. Here is a summary of the performance of each version of the model:

- **Version from Ref. [25]:** the adaptation of the standard model to a premixed case was capable of reproducing the main features of the mechanism of the light-round process. However, the τ_{LR} was $\sim 3-4$ times higher than the experimental one and did not follow the same trend with S_L. The only characteristic captured was the increase in τ_{LR} when moving the spark downstream.
- **Version 1:** including an enhancement term in particle velocity, based on flame propagation and dilatation had a positive impact on the simulations. The mechanism of burner-to-burner propagation and the ignition transient were still well captured by the code. Moreover, the main trends of τ_{LR} were now reproduced in the simulations, both in terms of correlation with S_L and spark location, while $\tau_{LR,sim}$ was $\sim 2\tau_{LR,exp}$. However, the test on a canonical case showed this version of the code did not properly reproduce the turbulent flame speed and its dependence on turbulence intensity.
- **Version 2:** the new definition of Ka_p based on the instantaneous velocity fluctuations experienced by the particles increased particle quenching during propagation. The result was an increase in stochasticity and less uniformity in the mechanism of propagation, while keeping the same key features observed in the experiments. This version of SPINTHIR was also capable of obtaining a realistic turbulent flame speed in the canonical case test. However, the τ_{LR} calculated from the simulations only partially improved compared to the standard version of the code. Namely, τ_{LR} decreased with S_L only for low values of laminar flame speed, and was $\sim 4-5$ times higher than the experimental evidence. In addition, a high number of simulations did not achieve light-round, a number far below the experimental evidence. This is due to the excessive quenching of the particles. The increase in ignition time associated with moving the spark away from the bluff body was positively reproduced.
- **Version 3:** implementing both modifications in the code affected both the propagation mechanism and the ignition time. The mechanism of light-round suffered from the combination of increased particle velocity and quenching. The main trend of τ_{LR} with S_L was correctly reproduced, however the differences between sparking at $x/D = 0.5$ and 5 were gradually lost. Moreover, the ignition time was still higher ($\sim 2-2.5$ times) than the experimental one and the decrease in number of failed light-rounds observed in version 2 was even amplified in version 3 by the enhancement of particle velocity (affecting Ka_p). In contrast with the mixed results on the annular geometry (which may also depend on the accuracy of the data coming from the cold flow CFD simulation), the canonical test showed this version well predicted the turbulent flame speed and its bending

behaviour with turbulence intensity.

Overall, the simulations show that the low-order model employed is capable of reproducing the key elements of flame propagation during the light-round transient. The versions of the code tested showed significant improvement and captured all qualitative trends seen in the experiment. Despite being less accuracy than an LES simulation in estimating light-round time for premixed annular chambers, the SPINTHIR model produces encouraging results, as the flame propagation and experimental trends were retrieved by the model, but for a tiny fraction of the computational cost of a LES of light-round.

4. Conclusions

This work explored the possibility to simulate the ignition transient and the light-round process in a premixed annular combustor using a stochastic low-order model, that included modifications to capture dilatation, turbulent flame propagation and local extinction. The aim of the study was to assess the reliability of the model on capturing the main features of flame propagation.

The simulations with the original model reproduced reasonably well the mechanism of flame propagation and its characteristics (i.e. initial flame growth, formation of two flame branches, pattern and direction of the light-round). However, the light-round time τ_{LR} was almost four times higher than in the experiments and the strong correlation between τ_{LR} and S_L was not captured. Therefore, in this work we included the laminar flame speed, unburnt over burnt gases density ratio and the particle instantaneous dynamics in the SPINTHIR model. The improved model reproduces the bending behaviour of turbulent flame speed with the ratio u'/S_L, therefore building confidence that it captures the fundamentals of turbulent premixed flame propagation.

When applied to the annular combustor, starting from a cold-flow CFD solution, the modifications proposed in this work showed a clear improvement to the model predictions, as now the important correlation between light-round time and laminar flame speed is captured. However, even if now the experimental trends are reproduced by the model, the light-round time is still overpredicted relative to the experimental measurements. We believe this is partly due to the different ways this quantity was evaluated in the experiments and in the simulations, and to the choice of relying on RANS steady-state CFD (which also impairs the results to some extent). Thus, further development is still needed to achieve an accurate estimation of light-round time. Nevertheless, the results reported in this study provide an improvement of the capability of this low-order modelling to simulate complex transient events, which is here assessed by the first time. Furthermore, this study highlights the importance of considering the laminar flame speed for the modelling of the flame particles' movement, as the updated model correctly reproduced the decreasing trend of light-round time with the increasing flame speed. Moreover, this study highlights a useful approach for assessing ignition in complex multi-burner combustion systems at low computational cost.

Acknowledgements

This work has received funding from the European Union's Horizon 2020 Research and Innovation Programme under the Marie Skłodowska-Curie Grant Agreement No.

765998 as part of project ANNULIGHT and from project PROTEUS from the Clean Sky Joint Undertaking (Agreement No. 785349).

Disclosure statement

No potential conflict of interest was reported by the authors.

Funding

R.C. has received funding from the European Union's Horizon 2020 Research and Innovation Programme under the Marie Skłodowska-Curie Grant Agreement No. 765998 as part of project "Annulight". L.C.C.M. has been supported by funding from the Clean Sky 2 Joint Undertaking (JU) under project PROTEUS, Grant Agreement No 785349. The JU receives support from the European Union's Horizon 2020 research and innovation programme and the Clean Sky 2 JU members other than the Union

References

[1] A.W. Lefebvre and D.R. Ballal, *Gas Turbine Combustion-Alternative Fuels and Emissions*, CRC press, Taylor and Francis group, NY, 2010.

[2] T.C. Lieuwen and V. Yang, *Gas Turbine Emissions*, Cambridge University Press, 2017.

[3] I. Glassman and R.A. Yetter, *Combustion*, Academic Press, 2008.

[4] E. Mastorakos, *Ignition of turbulent non-premixed flames*, Progress in Energy and Combustion Science 35 (2009), pp. 57–97, Available at http://dx.doi.org/10.1016/j.pecs.2008.07.002.

[5] E. Mastorakos, *Forced ignition of turbulent spray flames*, Proceedings of the Combustion Institute 36 (2017), pp. 2367–2383.

[6] J.F. Bourgouin, D. Durox, T. Schuller, J. Beaunier, and S. Candel, *Ignition dynamics of an annular combustor equipped with multiple swirling injectors*, Combustion and Flame 160 (2013), pp. 1398–1413, Available at http://dx.doi.org/10.1016/j.combustflame.2013.02.014.

[7] E. Machover and E. Mastorakos, *Experimental investigation on spark ignition of annular premixed combustors*, Combustion and Flame 178 (2017), pp. 148–157, Available at http://dx.doi.org/10.1016/j.combustflame.2017.01.013.

[8] Y. Xia, C. Linghu, Y. Zheng, C. Ye, C. Ma, H. Ge, and G. Wang, *Experimental Investigation of the Flame Front Propagation Characteristic During Light-round Ignition in an Annular Combustor*, Flow, Turbulence and Combustion (2019).

[9] R. Ciardiello, P.M. de Oliveira, A.W. Skiba, E. Mastorakos, and P.M. Allison, *Effect of spark location and laminar flame speed on the ignition transient of a premixed annular combustor*, Combustion and Flame 221 (2020), pp. 296 – 310, Available at http://www.sciencedirect.com/science/article/pii/S0010218020303163.

[10] E. Machover and E. Mastorakos, *Spark ignition of annular non-premixed combustors*, Experimental Thermal and Fluid Science 73 (2016), pp. 64–70, Available at http://dx.doi.org/10.1016/j.expthermflusci.2015.09.008.

[11] E. Machover and E. Mastorakos, *Experimental and numerical investigation on spark ignition of linearly arranged non-premixed swirling burners*, Combustion Science and Technology 189 (2017), pp. 1326–1353, Available at http://dx.doi.org/10.1080/00102202.2017.1294589.

[12] D. Barré, L. Esclapez, M. Cordier, E. Riber, B. Cuenot, G. Staffelbach, B. Renou, A. Vandel, L.Y. Gicquel, and G. Cabot, *Flame propagation in aeronautical swirled multi-*

burners: Experimental and numerical investigation, Combustion and Flame 161 (2014), pp. 2387–2405, Available at http://dx.doi.org/10.1016/j.combustflame.2014.02.006.

[13] J. Marrero-Santiago, A. Verdier, A. Vandel, G. Cabot, A.M. Boukhalfa, and B. Renou, *Effect of injector spacing in the light-around ignition efficiency and mechanisms in a linear swirled spray burner*, Heat and Mass Transfer 55 (2019), pp. 1871–1885, Available at https://doi.org/10.1007/s00231-018-2433-0.

[14] K. Prieur, D. Durox, J. Beaunier, T. Schuller, and S. Candel, *Ignition dynamics in an annular combustor for liquid spray and premixed gaseous injection*, Proceedings of the Combustion Institute 36 (2017), pp. 3717–3724, Available at http://dx.doi.org/10.1016/j.proci.2016.08.008.

[15] T. Lancien, K. Prieur, D. Durox, S. Candel, and R. Vicquelin, *Large Eddy Simulation of Light-Round in an Annular Combustor With Liquid Spray Injection and Comparison With Experiments*, Journal of Engineering for Gas Turbines and Power 140 (2017), p. 021504.

[16] K. Prieur, D. Durox, G. Vignat, T. Schuller, and S. Candel, *Flame and Spray Dynamics During the Light-Round Process in an Annular System Equipped With Multiple Swirl Spray Injectors*, ASME. Turbo Expo: Power for Land, Sea, and Air, Volume 4B: Combustion, Fuels, and Emissions 141 (2018).

[17] M. Boileau, G. Staffelbach, B. Cuenot, T. Poinsot, and C. Bérat, *LES of an ignition sequence in a gas turbine engine*, Combustion and Flame 154 (2008), pp. 2–22.

[18] M. Philip, M. Boileau, R. Vicquelin, E. Riber, T. Schmitt, B. Cuenot, D. Durox, and S. Candel, *Large eddy simulations of the ignition sequence of an annular multiple-injector combustor*, Proceedings of the Combustion Institute 35 (2015), pp. 3159 – 3166, Available at http://www.sciencedirect.com/science/article/pii/S1540748914003186.

[19] S. Puggelli, T. Lancien, K. Prieur, D. Durox, S. Candel, and R. Vicquelin, *Impact of Wall Temperature in Large Eddy Simulation of Light-Round in an Annular Liquid Fueled Combustor and Assessment of Wall Models*, in *Proceedings of the ASME Turbo Expo 2019: Turbomachinery Technical Conference and Exposition*, Vol. 4B: Combustion, Fuels, and Emissions, 06. 2019, Available at https://doi.org/10.1115/GT2019-91396.

[20] J. Marrero-Santiago, F. Collin-Bastiani, E. Riber, G. Cabot, B. Cuenot, and B. Renou, *On the mechanisms of flame kernel extinction or survival during aeronautical ignition sequences: Experimental and numerical analysis*, Combustion and Flame 222 (2020), pp. 70–84, Available at https://www.sciencedirect.com/science/article/pii/S0010218020303369.

[21] F. Collin-Bastiani, J. Marrero-Santiago, E. Riber, G. Cabot, B. Renou, and B. Cuenot, *A joint experimental and numerical study of ignition in a spray burner*, Proceedings of the Combustion Institute 37 (2019), pp. 5047–5055, Available at https://linkinghub.elsevier.com/retrieve/pii/S154074891830138X.

[22] Y. Tang, M. Hassanaly, V. Raman, B.A. Sforzo, S. Wei, and J.M. Seitzman, *Simulation of Gas Turbine Ignition Using Large Eddy Simulation Approach* (2018), p. 10.

[23] Y. Tang, M. Hassanaly, V. Raman, B.A. Sforzo, and J. Seitzman, *Probabilistic modeling of forced ignition of alternative jet fuels*, Proceedings of the Combustion Institute 38 (2021), pp. 2589–2596, Available at https://www.sciencedirect.com/science/article/pii/S1540748920304016.

[24] R. Saïd and R. Borghi, *A simulation with a "cellular automaton" for turbulent combustion modelling*, Symposium (International) on Combustion 22 (1989), pp. 569 – 577, Available at http://www.sciencedirect.com/science/article/pii/S0082078489800645.

[25] A. Neophytou, E.S. Richardson, and E. Mastorakos, *Spark ignition of turbulent recirculating non-premixed gas and spray flames: A model for predicting ignition probability*, Combustion and Flame 159 (2012), pp. 1503–1522, Available at http://dx.doi.org/10.1016/j.combustflame.2011.12.015.

[26] S.E. Richardson, *Ignition modelling for turbulent non-premixed flows*, PhD Thesis, University of Cambridge, Cambridge, UK, 2007.

[27] S.B. Pope, *Turbulent Flows*, Cambridge University Press, 2000.

[28] R.G. Abdel-Gayed, K.J. Al-Khishali, and D. Bradley, *Turbulent Burning Velocities and*

Flame Straining in Explosions, Proceedings of the Royal Society A: Mathematical, Physical and Engineering Sciences 391 (1984), pp. 393–414.

[29] S.F. Ahmed, R. Balachandran, T. Marchione, and E. Mastorakos, *Spark ignition of turbulent nonpremixed bluff-body flames*, Combustion and Flame 151 (2007), pp. 366–385.

[30] S.F. Ahmed, R. Balachandran, and E. Mastorakos, *Measurements of ignition probability in turbulent non-premixed counterflow flames*, Proceedings of the Combustion Institute 31 (2007), pp. 1507–1513.

[31] T. Marchione, S.F. Ahmed, and E. Mastorakos, *Ignition of turbulent swirling n-heptane spray flames using single and multiple sparks*, Combustion and Flame 156 (2009), pp. 166–180, Available at http://dx.doi.org/10.1016/j.combustflame.2008.10.003.

[32] A. Neophytou, E. Mastorakos, E. Richardson, S. Stow, and M. Zedda, *A practical model for the high-altitude relight of a gas turbine combustor*, in *Seventh Mediterranean Combustion Symposium (MCS-7) (10/09/11 - 14/09/11)*, September. 2011, Available at https://eprints.soton.ac.uk/384838/.

[33] T. Mosbach, R. Sadanandan, W. Meier, and R. Eggels, *Experimental Analysis of Altitude Relight Under Realistic Conditions Using Laser and High-Speed Video Techniques*, Turbo Expo: Power for Land, Sea, and Air Vol. 2: Combustion, Fuels and Emissions, Parts A and B, 06. 2010, pp. 523–532, Available at https://doi.org/10.1115/GT2010-22625.

[34] T. Soworka, M. Gerendas, R.L.G.M. Eggels, and E. Mastorakos, *Numerical Investigation of Ignition Performance of a Lean Burn Combustor at Sub-Atmospheric Conditions*, Proceedings of the ASME Turbo Expo 2014: Turbine Technical Conference and Exposition. Volume 4A: Combustion, Fuels and Emissions (2014), p. V04AT04A046, Available at https://doi.org/10.1115/GT2014-25644.

[35] M. Cordier, A. Vandel, B. Renou, G. Cabot, M.A. Boukhalfa, and M. Cazalens, *Spark ignition of confined swirled flames: experimental and numerical investigation*, in *Proceedings of ASME Turbo Expo*. 2013, pp. 1–12.

[36] M.P. Sitte, E. Bach, J. Kariuki, H.J. Bauer, and E. Mastorakos, *Simulations and experiments on the ignition probability in turbulent premixed bluff-body flames*, Combustion Theory and Modelling 20 (2016), pp. 548–565.

[37] E. Machover and E. Mastorakos, *Numerical Investigation of the Stochastic Behavior of Light-Round in Annular Non-Premixed Combustors*, Combustion Science and Technology 189 (2017), pp. 1467–1485.

[38] M. Cordier, A. Vandel, B. Renou, G. Cabot, M. Boukhalfa, L. Exclapez, D. Barré, E. Riber, B. Cuenot, and L. Gicquel, *Experimental and numerical analysis of an ignition sequence in a multiple-injector burner*, in *Proc ASME Turbo Exp 2013*. 2013, pp. GT2013–94681.

[39] K. Prieur, G. Vignat, D. Durox, T. Schuller, and S. Candel, *Flame and Spray Dynamics During the Light-Round Process in an Annular System Equipped With Multiple Swirl Spray Injectors*, Journal of Engineering for Gas Turbines and Power 141 (2019), Available at https://doi.org/10.1115/1.4042024, 061007.

[40] T. Lancien, K. Prieur, D. Durox, S. Candel, and R. Vicquelin, *Leading point behavior during the ignition of an annular combustor with liquid n-heptane injectors*, Proceedings of the Combustion Institute 37 (2019), pp. 5021 – 5029, Available at http://www.sciencedirect.com/science/article/pii/S1540748918301664.

[41] L. Esclapez, F. Collin-Bastiani, E. Riber, and B. Cuenot, *A statistical model to predict ignition probability*, Combustion and Flame 225 (2021), pp. 180–195, Available at https://www.sciencedirect.com/science/article/pii/S0010218020304715.

[42] R. Abdel-Gayed and D. Bradley, *Criteria for turbulent propagation limits of premixed flames*, Combustion and Flame 62 (1985), pp. 61 – 68, Available at http://www.sciencedirect.com/science/article/pii/0010218085900938.

[43] R. Ciardiello, R. Pathania, P. Allison, P.M. de Oliveira, and E. Mastorakos, *Ignition Probability and Lean Ignition Behaviour of a Swirled Premixed Bluff-Body Stabilised Annular Combustor*, Journal of Engineering for Gas Turbines and Power (2020), Available at https://doi.org/10.1115/1.4048461.

[44] R. Ciardiello, A.W. Skiba, R.L. Gordon, and E. Mastorakos, *Experimental assessment of the lean blow-off in a fully premixed annular combustor*, Experimental Thermal and Fluid Science 112 (2020), p. 109994, in press.

[45] N.A. Worth and J.R. Dawson, *Modal dynamics of self-excited azimuthal instabilities in an annular combustion chamber*, Combustion and Flame 160 (2013), pp. 2476–2489, Available at http://dx.doi.org/10.1016/j.combustflame.2013.04.031.

[46] M.S. Anand, R. Eggels, M. Staufer, M. Zedda, and J. Zhu, *An Advanced Unstructured-Grid Finite-Volume Design System for Gas Turbine Combustion Analysis*, Feb. American Society of Mechanical Engineers Digital Collection, 2014.

[47] J.F. Driscoll and C.C. Rasmussen, *Correlation and Analysis of Blowout Limits of Flames in High-Speed Airflows*, Journal of Propulsion and Power 21 (2008), pp. 1035–1044.

[48] J.F. Driscoll, J.H. Chen, A.W. Skiba, C.D. Carter, E.R. Hawkes, and H. Wang, *Premixed flames subjected to extreme turbulence: Some questions and recent answers*, Progress in Energy and Combustion Science 76 (2020), p. 100802, Available at http://www.sciencedirect.com/science/article/pii/S036012851930036X.

[49] A. Lipatnikov and J. Chomiak, *Turbulent flame speed and thickness: phenomenology, evaluation, and application in multi-dimensional simulations*, Progress in Energy and Combustion Science 28 (2002), pp. 1 – 74, Available at http://www.sciencedirect.com/science/article/pii/S0360128501000077.

[50] G. Nivarti and S. Cant, *Direct numerical simulation of the bending effect in turbulent premixed flames*, Proceedings of the Combustion Institute 36 (2017), pp. 1903 – 1910, Available at http://www.sciencedirect.com/science/article/pii/S1540748916303340.